

The Transient Response of the Southern Ocean to Stratospheric Ozone Depletion

3 William J. M. Seviour*, Anand Gnanadesikan, Darryn W. Waugh

⁴ Department of Earth and Planetary Sciences, Johns Hopkins University, Baltimore, Maryland.

⁵ *Corresponding author address: William Seviour, Department of Earth and Planetary Sciences,
⁶ Johns Hopkins University, 3400 N. Charles St., Baltimore, MD, 21218.
⁷ E-mail: wseviou1@jhu.edu

ABSTRACT

Recent studies have suggested that the response of the Southern Ocean to stratospheric ozone depletion is nonmonotonic in time; consisting of an initial cooling followed by a long-term warming. This result may be significant for the attribution of observed Southern Ocean temperature and sea ice trends, but the time scale and magnitude of the response is poorly constrained, with a wide spread among climate models. Furthermore, a long-lived initial cooling period has only been observed in a model with idealized geometry and lacking an explicit representation of ozone. Here we calculate the transient response of the Southern Ocean to a step-change in ozone in a comprehensive coupled climate model, GFDL ESM2Mc. The Southern Ocean responds to ozone depletion with an initial cooling, lasting 25 years, followed by a warming. We extend previous studies to investigate the dependence of the response on the ozone forcing as well as the regional pattern of this response. The response of the Southern Ocean relative to natural variability is shown to be largely independent of the initial state. However, the magnitude of this response is much less than that of natural variability found in the model, which limits its influence and detectability.

25 **1. Introduction**

26 In recent decades significant trends in the summertime atmospheric circulation over the South-
27 ern Ocean (SO) have been observed. The extratropical jet has shifted poleward and intensified
28 (Marshall 2003; Thompson et al. 2011), consistent with a more positive Southern Annular Mode
29 (SAM). These trends are outside the range of natural variability found in coupled climate models
30 (Thomas et al. 2015), and have been largely attributed to the impact of stratospheric ozone de-
31 pletion (Polvani et al. 2011; Gerber and Son 2014). At the same time, an increase in Southern
32 Hemisphere sea ice cover has been observed (Comiso and Nishio 2008; Parkinson and Cavalieri
33 2012), most prominent in the fall, and in contrast to the large decrease seen in the Arctic.

34 Several studies have investigated a possible link between these atmospheric and ocean–sea ice
35 trends. The sea surface temperature (SST) pattern associated with interannual variability in the
36 SAM is a dipole in the meridional direction, a feature driven largely by horizontal Ekman transport,
37 and consistent across observations and climate models (Watterson 2000; Hall and Visbeck 2002;
38 Sen Gupta and England 2006; Ciasto and Thompson 2008). For the positive phase of the SAM,
39 this pattern gives a warming in SST at about 40°S and cooling south of about 50°S, leading to an
40 overall increase in SO sea ice cover (Lefebvre et al. 2004; Lefebvre and Goosse 2008). Following
41 these results, Goosse et al. (2009) argued that the ozone-driven trend toward a more positive SAM
42 is the main driver of the observed SO sea ice expansion. However, this contradicts the results of
43 many coupled climate model studies which have found a warming of the SO and a reduction in
44 sea ice extent associated with stratospheric ozone depletion (Sigmond and Fyfe 2010; Bitz and
45 Polvani 2012; Smith et al. 2012; Sigmond and Fyfe 2014; Previdi et al. 2014).

46 Ferreira et al. (2015) (hereafter F15) attempted to reconcile these opposing views by proposing
47 that the response of the SO to stratospheric ozone depletion has two time scales; a fast and slow

48 response. They found the fast response to be similar to the interannual SAM-SST correlation,
49 driven by horizontal Ekman transport, and leading to an increase in sea ice cover. On the other
50 hand, the slow response was shown to be driven by upwelling of warm water from below the
51 mixed layer, leading to a reduction in sea ice cover, and consistent with coupled climate modeling
52 studies. F15 computed the transient ocean response to a step function in ozone depletion in two
53 coupled climate models: the MITgcm and CCSM3.5. These two simulations had very different
54 configurations, with the MITgcm using an idealized geometry (Double-Drake), and without an
55 explicit representation of ozone, while CCSM3.5 is a more comprehensive coupled model with
56 explicit ozone, realistic geometry, and more sophisticated radiation and cloud schemes. While
57 F15 showed both models to give a two time scale response, there were also significant differences
58 between the simulations. The initial cooling period was about 20 years in the MITgcm, but just 5
59 years in CCSM3.5. Furthermore, the magnitude of the cooling was around three times greater in
60 the MITgcm than CCSM3.5.

61 More recently, Kostov et al. (2016) investigated the response of the SO to a step increase in the
62 SAM by studying lagged correlations in preindustrial control simulations included in the Coupled
63 Model Intercomparison Project Phase 5 (CMIP5). They found a wide range of responses, with
64 some models giving a two time scale response, but others with persistent cooling. Among those
65 models which did show a two time scale response there was a wide range of times at which SST
66 anomalies cross from negative to positive. Better constraining the time scales and magnitudes of
67 this response will be crucial in determining how much (if any) of the observed sea ice trends may
68 be attributed to ozone depletion, as well as how ozone recovery may influence future SO changes.

69 In this study, we calculate the transient response of the Southern Ocean to stratospheric ozone
70 depletion in the Geophysical Fluid Dynamics Laboratory (GFDL) Earth System Model with Mod-
71 ular Ocean Model (ESM2Mc) coupled climate model. We find an initial cooling lasting about

⁷² 25 years, followed by a warming, and a similar magnitude found by F15 for the MITgcm. This
⁷³ demonstrates that a long-lived cooling such as found for the MITgcm is possible in a climate model
⁷⁴ with realistic geometry and explicitly represented ozone. However, this response is small relative
⁷⁵ to the natural variability of the model, and only clearly emerges in an ensemble of simulations.
⁷⁶ We extend F15 to investigate how the response depends on the prescribed ozone forcing and the
⁷⁷ initial conditions. We also investigate the spatial structure of the response, showing that both the
⁷⁸ time scales and magnitudes of the response vary over the SO.

⁷⁹ **2. Ozone Response Simulations**

⁸⁰ We calculate the response of the SO to a step-change in stratospheric ozone depletion, an ap-
⁸¹ proach described in general terms by Marshall et al. (2014). An advantage of calculating this
⁸² response is that linear theory allows the step-function response to be used to predict the response
⁸³ to an arbitrary time-varying forcing. We use the GFDL ESM2Mc model (Gnanadesikan et al.
⁸⁴ 2015), a coarse-resolution version of GFDL ESM2M (Dunne et al. 2012). The model consists of
⁸⁵ a $3.875^\circ \times 3^\circ$ latitude-longitude atmosphere with 24 vertical levels, coupled to a $3^\circ \times 1.5^\circ$ ocean
⁸⁶ model with 28 vertical levels. In the ocean model, advection due to geostrophic eddies is param-
⁸⁷ eterized using a shear-dependent mixing coefficient (Gent and Mcwilliams 1990), as well as a
⁸⁸ lateral eddy mixing coefficient (Redi 1982), A_{Redi} , with a global value of $800 \text{ m}^2 \text{ s}^{-1}$.

⁸⁹ Initial conditions for our simulations are taken from a 500-year-long preindustrial control sim-
⁹⁰ ulation using a global carbon dioxide concentration of 286 ppm and ozone concentrations for the
⁹¹ year 1860 from the Stratosphere-troposphere Processes and their Role in Climate (SPARC) dataset
⁹² (Cionni et al. 2011). We then instantaneously impose a change to contemporary ozone concentra-
⁹³ tions, using a climatology from 1995-2001. These contemporary concentrations are derived from
⁹⁴ a specified dynamics version of the Whole Atmosphere Community Climate Model (WACCM-

SD), in which temperatures and winds are nudged to meteorological assimilation analysis results, but chemistry calculated interactively (Solomon et al. 2015). Neely et al. (2014) have proposed that the coarse temporal resolution (monthly-mean) of prescribed ozone used by many simulations leads to an underestimate of the magnitude of ozone depletion. In order to test this, we impose daily-mean concentrations in half of the simulations, and monthly means of these daily values in the other half. The seasonal cycle of polar cap (70° - 90° N) column ozone for these imposed ozone concentrations are shown in Figure 1. Ozone is reduced relative to preindustrial concentrations throughout the year, but the largest difference seen to occur in the spring (September–November), and the minimum around October 1st is less pronounced for the monthly-mean ozone than daily-mean because of the linear interpolation used.

The SO in GFDL ESM2Mc displays significant multi-decadal variability, a feature seen in several, but not all, coupled climate models (de Lavergne et al. 2014; Martin et al. 2013). Figure 2 shows the time series of SO SST for 200 years of the preindustrial control simulation. Multi-decadal variability is apparent, with a period of approximately 50 years and this variability is dominated by the Ross and Weddell seas (Figure 2(b)). Further investigation shows this variability to be predominantly caused by large deep convective events in these regions, as was previously reported by (Galbraith et al. 2011) in a similar model. We test the dependence of the SO response to ozone depletion on the initial conditions by initializing half of the ozone response simulations with relatively cold SO SST ('cold start') and half relatively warm ('warm start'), as illustrated in Figure 2(a). These initialization dates are clustered around two warm and cold periods, and spaced 5 years apart within each period. Testing the dependence of this response on initial conditions is particularly important because the ability to reconstruct the response to an arbitrary forcing from the step-function response relies on linear theory. A necessary condition of the response being linear is that it is independent of the initial conditions.

119 In total, we run 24 ozone response simulations, each 48 years long. These are divided into
120 12 start dates (6 warm start and 6 cold start), with one daily-mean ozone and one monthly-mean
121 ozone simulation initialized on each date. We begin by discussing the ensemble mean response
122 before describing the effects of the differences in ozone forcing and the initial state.

123 **3. Results**

124 *a. Ensemble Mean Response*

125 Ozone depletion is seen to cause a rapid increase in zonal wind stress poleward of the clima-
126 tological maximum, and a small decrease equatorward of it (Figure 3). This is indicative of a
127 poleward shift and intensification of the extratropical jet, seen in both observations over the past
128 few decades (Thompson and Solomon 2002) and climate model simulations of ozone depletion
129 (Gerber and Son 2014). The ensemble mean maximum wind stress anomaly is about 7 mPa,
130 which is less than the 12 mPa found by F15 for both the MITgcm and CCSM3.5. Although a clear
131 increase in wind stress is seen between 50°-65°S, there is also a large amount of variability, even
132 in the ensemble mean (Figure 3(b)). This increase is also not zonally symmetric, with the largest
133 anomalies in the Indian Ocean sector, and weaker values near Western Antarctica.

134 This atmospheric response to ozone depletion leads to a response in the SO. Figure 4 shows the
135 ensemble mean response of zonal mean SST following the introduction of ozone depletion. Here
136 anomalies are calculated as the difference from the climatology of the control simulation. The
137 initial response (years 0-25) consists of a dipole, with cooling between 50°-70°S and warming
138 from 50°-35°S, a pattern which resembles the SST signature of a positive SAM on interannual
139 time scales (Watterson 2000). After 25 years the structure of this response changes significantly,
140 to become a monopole, with warming present throughout the region, though it is particularly

¹⁴¹ strong near the Antarctic continent (70°S). This response greatly resembles that found by F15 for
¹⁴² the MITgcm (see their Figure 5), which switches from a dipole to monopole pattern after about 20
¹⁴³ years.

¹⁴⁴ The ocean response is not limited to the surface. Figure 5 shows the ensemble mean evolution
¹⁴⁵ of SO temperature with depth following the introduction of ozone depletion. The initial cooling
¹⁴⁶ is confined near the surface but a warming of the subsurface is present from the start of the sim-
¹⁴⁷ ulation, growing deeper with time. The SST warming at about 25 years occurs when this warm
¹⁴⁸ subsurface water is entrained into the mixed layer.

¹⁴⁹ The anomalous wind stress shown in Figure 3 also drives an anomalous ocean circulation. Fig-
¹⁵⁰ ure 6(a) shows the Eulerian meridional overturning circulation response to ozone depletion. This
¹⁵¹ anomalous circulation consists of two cells which closely match the regions of positive and nega-
¹⁵² tive surface wind stress anomalies, with clockwise circulation from approximately 65° - 55°S and
¹⁵³ counter-clockwise from 55° - 30°S . The Eulerian MOC streamlines are approximately vertical in
¹⁵⁴ the interior (as expected by geostrophy), with return flow in the top and bottom Ekman layers. The
¹⁵⁵ equatorward cell has deeper return flow, permitted by the meridional barriers in this region.

¹⁵⁶ It is not the Eulerian, but the residual circulation (sum of Eulerian and eddy-induced parame-
¹⁵⁷ terized circulations), which determines the transport of heat. This residual circulation is shown
¹⁵⁸ alongside the Eulerian circulation in Figure 6(b). The maximum anomaly in the residual circu-
¹⁵⁹ lation at about 57°S is significant, being about 75% of the interannual standard deviation of the
¹⁶⁰ control simulation at the same location. Relative to the Eulerian circulation, the eddy-induced cir-
¹⁶¹ culation is seen to narrow the region of anomalous upwelling (indicated by a positive meridional
¹⁶² gradient in Ψ'_{Res}) to between approximately 67° - 57°S , as well as significantly strengthening the
¹⁶³ upwelling in this region. Although these circulations are only shown at 200 m, the results are not
¹⁶⁴ highly depth-dependent below the mixed layer.

165 Ocean temperature increases upward poleward of about 55°S (Figure 6(a)) because of the pres-
166 ence of seasonal sea ice. The upwelling in this region is therefore expected to result in a warming.
167 Figure 7 shows the temperature response in this upwelling region, near 62°S and 200 m depth
168 (similar results are found at other locations in the upwelling region). Indeed, a fairly linear in-
169 crease in temperature can be seen over the length of the simulation. It should be noted, however,
170 that vertical advection is not the sole driver of this temperature trend, and that vertical mixing
171 also plays an important role. More detailed analysis of the physical mechanisms driving this re-
172 sponse will be the subject of a future study. Can this subsurface temperature trend explain the SST
173 warming after about 25 years (Figure 2)? The average initial (0-20 years) SST response between
174 50-70°S is about -0.1 K. If these subsurface temperatures are efficiently entrained into the mixed
175 layer, we might expect this initial cooling to be offset when subsurface anomalies reach $+0.1$ K.
176 This occurs at about 21 years (Figure 7), so there is relatively good agreement in these time scales.

177 *b. Influence of the Temporal Resolution of Ozone Forcing*

178 Figure 3 shows that the maximum annual mean wind stress anomaly increases by approximately
179 50% on changing from monthly- to daily-mean ozone. In agreement with Neely et al. (2014), this
180 indicates that linear interpolation between monthly-mean values, such as was used for the majority
181 of models which contributed to CMIP5 (Gerber and Son 2014), significantly underestimates the
182 effects of ozone depletion. Figure 3 also shows that the mean windstress anomalies are similar
183 for the cold start and warm start simulation, indicating that the atmospheric response is largely
184 independent of the initial ocean state.

185 The difference between simulations with monthly- and daily-mean ozone is not limited to the
186 atmosphere. Figure 6(b) shows the Eulerian streamfunction at 200 m for the daily- and monthly-
187 mean ozone simulations. There is an approximately 50% increase in the anomalous circulation

188 on changing from monthly- to daily-mean ozone, indicating that the effect of the temporal res-
189 olution of ozone extends to the ocean interior. However, the difference between the daily- and
190 monthly-mean ozone simulations is much reduced in the residual-mean circulation, indicating
191 that parameterized eddies are acting to compensate this difference in the Ekman upwelling. Since
192 the residual circulation determines the transport of heat, we might therefore expect similar temper-
193 ature responses for the monthly- and daily-mean ozone simulations. Indeed, there is no significant
194 difference in their temperature trends, as can be seen in Figure 7.

195 We have seen that the differences in ozone forcing lead to a significantly different atmospheric
196 response and Eulerian ocean circulation. However, the effect of parameterized eddies is to reduce
197 these differences, leading to a similar subsurface temperature response. The SST responses in the
198 daily- and monthly-mean ozone simulations are also similar (Figure 8), and their differences are
199 dwarfed by those between the warm and cold-start simulations.

200 *c. Influence of the Initial State*

201 Figure 8 demonstrates the importance of the initial state in the ozone response simulations; those
202 simulations initialized with relatively warm SST cool over the first 25 years, while those initialized
203 with cold SST warm. Moreover, both warm- and cold-start simulations show reversals of these
204 trends around 25-30 years. It is not clear from this figure which part of this behavior is natural
205 (i.e., unforced), and which, if any, is a forced response to ozone depletion. In order to determine
206 this we study the difference of the ozone response simulations from the path of natural variability.

207 This path of natural variability could simply be taken to be that of the control simulation, how-
208 ever, because of the chaotic nature of SST evolution, the control simulation represents just one
209 instance of a distribution of possible paths. Using this single control simulation path therefore
210 introduces a large amount of noise into the results, which rapidly swamps any signal. Instead

we aim to determine the path of natural variability from the autocorrelation function of SST over the 500-year control simulation. This autocorrelation function multiplied by the initial SST then gives the *expected* path of natural variability of an ensemble initialized with that value. In order to test this method we select from the control simulation a set of 21 years with warm and cold SO SST, each of which must be at least one standard deviation from the mean, and spaced at least 5 years apart, to mirror the initialization of the ozone response simulations. The average of the SST evolution following these years is shown as the dashed lines in Figure 9. As well as this, the path determined by autocorrelation is shown, along with a 95% uncertainty range due to the finite length of the control simulation. The dashed lines almost always lie within the uncertainty range for the autocorrelation, showing that the autocorrelation accurately captures the unforced SST evolution.

The evolution of SST over the SO, Ross Sea, and Weddell Sea following ozone depletion for the warm- and cold-start ensembles is shown in Figure 10. Also shown is the path of natural variability (left) and the difference between this response and natural variability (right). In the majority of cases natural variability is seen to explain the most of the SST evolution, with the SST response falling within the uncertainty range of natural variability (shaded regions). A clear exception to this is the Ross Sea, particularly the warm start ensemble, which warms strongly after 15 years, in contrast to the cooling trend of natural variability.

Differences of the forced response from natural variability (Figure 10, right) show similar forced responses regardless of the initial conditions, although there is a large amount of variability. In almost all cases there is an initial cooling followed by a warming, with the exception of the cold start ensemble over the SO, which maintains negative anomalies throughout the length of the simulation. There is also a relatively large difference between the warm and cold start simulations over the Ross Sea after 30 years, although both show positive anomalies. Importantly, in order to

235 calculate the response to a time-varying forcing from the step function response it is a necessary
236 condition that this response be independent of the initial conditions. This result therefore supports
237 the step function response approach (Marshall et al. 2014) for predicting the response to a more
238 realistic ozone forcing. Most of the simulations show a decrease in SST anomalies after about 40
239 years. This indicates that the SO may not stabilize at a warmer temperature in our simulations,
240 as found by F15, but rather continues to vary periodically. The forced response may therefore be
241 thought of as a modulation of natural variability. Future investigation will aim to better understand
242 this result.

243 Figure 10 shows some significant regional differences in the forced response to ozone depletion.
244 First, although natural variability is larger in the Weddell Sea, the Ross Sea shows a stronger
245 forced response, particularly in the long-term warming. Second, the time scales of the transient
246 response are regionally dependent; the initial cooling lasts about 15 years in the Ross Sea, and
247 about 30 years in the Weddell Sea. These regional differences in the SST response are further
248 illustrated in Figure 11, which shows maps of SST anomaly over three 15-year periods following
249 the introduction of ozone depletion. The Ross Sea is seen to warm in both the warm- and cold-start
250 ensembles, while the Weddell Sea cools in the warm start ensemble, and warms in the cold start
251 ensemble. The net result is that the warm-start ensemble results in a dipole of SST after 15 years,
252 while the cold start shows warming throughout the SO. In the ensemble average, the dominant
253 long-term warming signal is seen to be in the Ross Sea.

254 Sea ice changes largely follow the SST patterns discussed above (Figure 12). In the ensemble
255 mean, there is little change in sea ice concentrations over the first 15 years, while differences
256 between the warm- and cold-start simulations are dominated by the Weddell Sea. The long-term
257 response gives a reduction in sea ice concentrations in the Ross Sea in all cases, with opposite

258 responses of the Weddell Sea for warm- and cold-start simulations and little overall change in the
259 ensemble mean.

260 Changes in winter and summer sea ice area are shown in Figure 13. In the ensemble mean, the
261 area does not change much in either case for the first 20-25 years, but then falls to a minimum at
262 about 30 years, before increasing again. The peak fractional change in sea ice area is about 10%
263 in winter and 20% during the summer, the larger fractional summer change coming at the time of
264 the largest ozone-induced atmospheric anomalies (Thompson et al. 2011). These changes in sea
265 ice extent are largely consistent with SO SST (Figure 10), although there is not an initial increase
266 in sea ice, as might be expected from the initial cooling of SST. This is because the largest initial
267 SST cooling in the ensemble mean is quite far equatorward in the Ross Sea sector (Figure 11,
268 top-left), away from the sea ice edge, and so has little effect on sea ice in this region (Figure 12,
269 top-left). The recovery of sea ice after 30 years again demonstrates that the SO continues to vary
270 periodically, rather than stabilizing at a new mean value.

271 **4. Conclusions**

272 In this study we have investigated the transient response of the SO to a step change in strato-
273 spheric ozone depletion, using a comprehensive coupled climate model, GFDL ESM2Mc. The
274 main conclusions are as follows:

- 275 1. Ozone depletion causes a poleward shift of the extratropical jet, leading to enhanced zonal
276 wind stress over much of the SO. Consistent with Neely et al. (2014), we find an approxi-
277 mately 50% increase in the maximum annual-mean wind stress anomaly on changing from
278 monthly-mean to daily ozone. This indicates that linear interpolation between monthly mean
279 values, which fails to capture the sharp ozone minimum near October 1st (Figure 1), leads to a
280 significant underestimate of the effects of ozone depletion. The effect of the temporal resolu-

tion of prescribed ozone is not limited to the atmosphere; the stronger wind stress anomalies using daily ozone drive a stronger Eulerian MOC relative to monthly-mean ozone. However, when considering the residual circulation, which includes the effect of parameterized eddies, this difference is much reduced. Since the residual circulation determines the advection of heat, there is little difference in ocean temperature between monthly-mean and daily ozone simulations.

2. Following the introduction of ozone depletion, the SO SST cools and then warms after about 25 years, similar to the result found by F15 for the MITgcm. However, in contrast to the idealized geometry set-up used by F15, we are able to determine the regional responses to ozone depletion. The longest-lived initial cooling is found in the Weddell Sea, while the largest warming is in Ross Sea. Observed SO trends over the last 30 years have been highly regionally dependent (Parkinson and Cavalieri 2012), and this further highlights the need to study regional responses. Future work will aim to understand the dynamics driving these different regional responses.

3. GFDL ESM2Mc displays significant quasi-periodic natural variability, driven by SO deep convective events, which is necessary to remove in order to determine the forced response. After removing this natural variability the response is seen to be largely independent of the initial conditions (Figure 10). This result is important because in order to construct the response to an arbitrary forcing from the step response, it is necessary that this response be independent of the initial conditions (Marshall et al. 2014).

F15 suggested that ozone depletion could have contributed to the observed expansion of sea ice cover around Antarctica in the last three decades (Parkinson and Cavalieri 2012). Indeed, given the initial 25-year cooling seen in this study, our results would seem to support their conclusions.

304 However, it should be noted that the magnitude of the forced SO SST response found here is small
305 compared to natural variability. The initial annual-mean SO cooling found here is about 0.1 K, but
306 the interannual standard deviation of SO SST in GFDL ESM2Mc is 0.4 K. Hence, it would take
307 approximately 20 years to detect this forced signal (at the 95% confidence level, using a two-tailed
308 *t*-test), which is not much less than the duration of the signal itself. The time required to detect
309 the response to a realistic ozone forcing, rather than a step-function change would be even longer
310 than this. The interannual standard deviation of SO SST in the MITgcm simulation analyzed by
311 F15 is similar to that of GFDL ESM2Mc (David Ferreira, pers. comm.), though it is less periodic.
312 The magnitude of the forced response is also similar, hence we might expect a similar time scale
313 to detect a signal in the MITgcm. This result highlights the importance of better constraining the
314 magnitudes of both the SO forced response and natural variability for the attribution of observed
315 trends.

316 *Acknowledgments.* This work was funded by a Frontiers of Earth System Dynamics grant from
317 the US National Science Foundation (FESD-1338814). We thank Doug Kinnison for providing
318 the WACCM-SD ozone data.

319 References

- 320 Bitz, C. M., and L. M. Polvani, 2012: Antarctic climate response to stratospheric ozone de-
321 pletion in a fine resolution ocean climate model. *Geophys. Res. Lett.*, **39**, L20705, doi:
322 10.1029/2012GL053393.
- 323 Ciasto, L. M., and D. W. J. Thompson, 2008: Observations of large-scale ocean-atmosphere inter-
324 action in the Southern Hemisphere. *J. Clim.*, **21**, 1244–1259, doi:10.1175/2007JCLI1809.1.

- 325 Cionni, I., and Coauthors, 2011: Ozone database in support of CMIP5 simulations: results
326 and corresponding radiative forcing. *Atmos. Chem. Phys.*, **11**, 11 267–11 292, doi:10.5194/
327 acp-11-11267-2011.
- 328 Comiso, J. C., and F. Nishio, 2008: Trends in the sea ice cover using enhanced and compat-
329 ible AMSR-E, SSM/I, and SMMR data. *J. Geophys. Res. Ocean.*, **113**, 1–22, doi:10.1029/
330 2007JC004257.
- 331 de Lavergne, C., J. B. Palter, E. D. Galbraith, R. Bernardello, and I. Marinov, 2014: Cessation of
332 deep convection in the open Southern Ocean under anthropogenic climate change. *Nat. Clim.
333 Chang.*, **4**, 278–282, doi:10.1038/nclimate2132.
- 334 Dunne, J. P., and Coauthors, 2012: GFDL’s ESM2 Global Coupled Climate-Carbon Earth System
335 Models. Part I: Physical Formulation and Baseline Simulation Characteristics. *J. Clim.*, **25**,
336 6646–6665, doi:10.1175/JCLI-D-11-00560.1.
- 337 Ferreira, D., J. Marshall, C. M. Bitz, S. Solomon, and A. Plumb, 2015: Antarctic Ocean and
338 Sea Ice Response to Ozone Depletion: A Two-Time-Scale Problem. *J. Clim.*, **28**, 1206–1226,
339 doi:10.1175/JCLI-D-14-00313.1.
- 340 Galbraith, E. D., and Coauthors, 2011: Climate Variability and Radiocarbon in the CM2Mc Earth
341 System Model. *J. Clim.*, **24**, 4230–4254, doi:10.1175/2011JCLI3919.1.
- 342 Gent, P. R., and J. C. Mcwilliams, 1990: Isopycnal Mixing in Ocean Circulation Models. *J. Phys.
343 Oceanogr.*, **20**, 150–155, doi:10.1175/1520-0485(1990)020<0150:IMIOCM>2.0.CO;2.
- 344 Gerber, E. P., and S.-W. Son, 2014: Quantifying the Summertime Response of the Austral Jet
345 Stream and Hadley Cell to Stratospheric Ozone and Greenhouse Gases. *J. Clim.*, **27 (14)**, 5538–
346 5559, doi:10.1175/JCLI-D-13-00539.1.

- 347 Gnanadesikan, A., M.-A. Pradal, and R. Abernathey, 2015: Isopycnal mixing by mesoscale eddies
348 significantly impacts oceanic anthropogenic carbon uptake. *Geophys. Res. Lett.*, **42**, 4249–4255,
349 doi:10.1002/2015GL064100. Received.
- 350 Goosse, H., W. Lefebvre, A. de Montety, E. Crespin, and A. H. Orsi, 2009: Consistent past half-
351 century trends in the atmosphere, the sea ice and the ocean at high southern latitudes. *Clim.
352 Dyn.*, **33**, 999–1016, doi:10.1007/s00382-008-0500-9.
- 353 Hall, A., and M. Visbeck, 2002: Synchronous Variability in the Southern Hemisphere Atmosphere
354 , Sea Ice , and Ocean Resulting from the Annular Mode. *J. Clim.*, **15**, 3043–3057, doi:10.1175/
355 1520-0442(2002)015<3043:SVITSH>2.0.CO;2.
- 356 Kostov, Y., J. Marshall, U. Hausmann, K. C. Armour, D. Ferreira, and M. M. Holland, 2016: Fast
357 and slow responses of the Southern Ocean sea surface temperature to SAM in coupled climate
358 models. *Clim. Dyn.*, In review.
- 359 Lefebvre, W., and H. Goosse, 2008: An analysis of the atmospheric processes driving the large-
360 scale winter sea ice variability in the Southern Ocean. *J. Geophys. Res.*, **113**, C02 004, doi:
361 10.1029/2006JC004032.
- 362 Lefebvre, W., H. Goosse, R. Timmermann, and T. Fichefet, 2004: Influence of the Southern
363 Annular Mode on the sea ice–ocean system. *J. Geophys. Res.*, **109**, C09 005, doi:10.1029/
364 2004JC002403.
- 365 Marshall, G. J., 2003: Trends in the southern annular mode from observations and reanalyses. *J.
366 Clim.*, **16**, 4134–4143.
- 367 Marshall, J., K. C. Armour, J. R. Scott, Y. Kostov, U. Hausmann, D. Ferreira, T. G. Shep-
368 herd, and C. M. Bitz, 2014: The ocean’s role in polar climate change: asymmetric Arc-

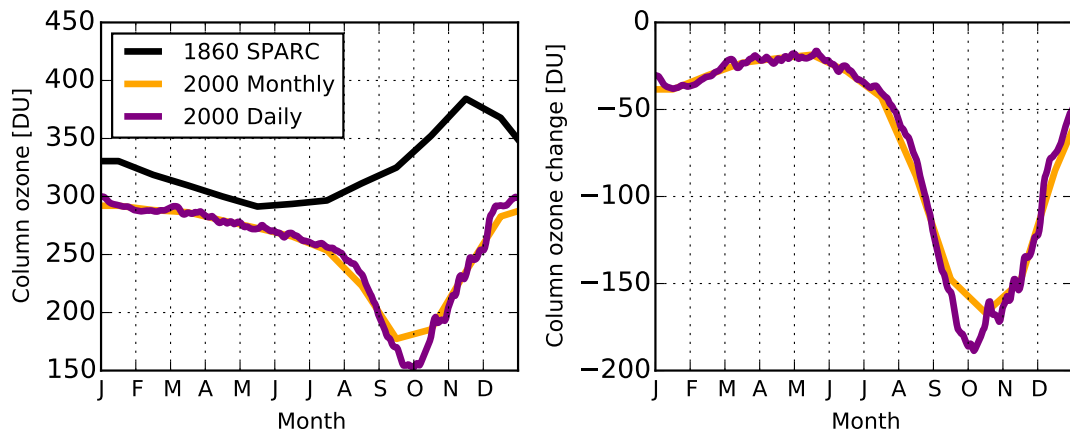
- tic and Antarctic responses to greenhouse gas and ozone forcing. *Philos. Trans. R. Soc. A*, **372**, 20130 040, doi:10.1098/rsta.2013.0040, URL <http://rsta.royalsocietypublishing.org/content/372/2019/20130040.full.html{\#}ref-list-1>.
- Martin, T., W. Park, and M. Latif, 2013: Multi-centennial variability controlled by Southern Ocean convection in the Kiel Climate Model. *Clim. Dyn.*, **40**, 2005–2022, doi:10.1007/s00382-012-1586-7.
- Neely, R. R., D. R. Marsh, K. L. Smith, S. M. Davis, and L. M. Polvani, 2014: Biases in southern hemisphere climate trends induced by coarsely specifying the temporal resolution of stratospheric ozone. *Geophys. Res. Lett.*, **41**, doi:10.1002/2014GL061627.
- Parkinson, C. L., and D. J. Cavalieri, 2012: Antarctic sea ice variability and trends, 1979-2010. *Cryosph.*, **6**, 871–880, doi:10.5194/tc-6-871-2012.
- Polvani, L. M., D. W. Waugh, G. J. P. Correa, and S.-W. Son, 2011: Stratospheric Ozone Depletion: The Main Driver of Twentieth-Century Atmospheric Circulation Changes in the Southern Hemisphere. *J. Clim.*, **24**, 795–812, doi:10.1175/2010JCLI3772.1.
- Previdi, M., L. M. Polvani, and M. Previdi, 2014: Climate system response to stratospheric ozone depletion and recovery. *Q. J. R. Meteorol. Soc. Q. J. R. Meteorol. Soc.*, **140**, 2401–2419, doi:10.1002/qj.2330.
- Redi, M., 1982: Oceanic isopycnal mixing by coordinate rotation. *J. Phys. Oceanogr.*, **12**, 1154–1158, doi:10.1175/1520-0485(1983)013<1318:OIMBCR>2.0.CO;2.
- Sen Gupta, A., and M. H. England, 2006: Coupled ocean-atmosphere-ice response to variations in the southern annular mode. *J. Clim.*, **19**, 4457–4486, doi:10.1175/JCLI3843.1, JCLI3843.1/JCLI3843.1.

- 391 Sigmond, M., and J. C. Fyfe, 2010: Has the ozone hole contributed to increased Antarctic sea ice
392 extent? *Geophys. Res. Lett.*, **37**, L18 502, doi:10.1029/2010GL044301.
- 393 Sigmond, M., and J. C. Fyfe, 2014: The Antarctic Sea Ice Response to the Ozone Hole in Climate
394 Models. *J. Clim.*, **27**, 1336–1342, doi:10.1175/JCLI-D-13-00590.1.
- 395 Smith, K. L., L. M. Polvani, and D. R. Marsh, 2012: Mitigation of 21st century Antarctic
396 sea ice loss by stratospheric ozone recovery. *Geophys. Res. Lett.*, **39**, L20 701, doi:10.1029/
397 2012GL053325.
- 398 Solomon, S., D. Kinnison, J. Bandoro, and R. Garcia, 2015: Simulation of polar ozone depletion:
399 An update. *J. Geophys. Res.*, **120**, 7958–7974, doi:10.1002/2015JD023365.
- 400 Thomas, J. L., D. Waugh, and A. Gnanadesikan, 2015: Decadal variability in the Southern Hemi-
401 sphere extratropical circulation: Recent trends and natural variability. *Geophys. Res. Lett.*, **42**,
402 5508–5515, doi:10.1002/2015GL064521.
- 403 Thompson, D. W. J., and S. Solomon, 2002: Interpretation of recent Southern Hemisphere climate
404 change. *Science*, **296**, 895–899, doi:10.1126/science.1069270.
- 405 Thompson, D. W. J., S. Solomon, P. J. Kushner, M. H. England, K. M. Grise, and D. J. Karoly,
406 2011: Signatures of the Antarctic ozone hole in Southern Hemisphere surface climate change.
407 *Nat. Geosci.*, **4**, 741–749, doi:10.1038/ngeo1296.
- 408 Watterson, I. G., 2000: Southern midlatitude zonal wind vacillation and its interaction with the
409 ocean in GCM simulations. *J. Clim.*, **13**, 562–578, doi:10.1175/1520-0442(2000)013<0562:
410 SMZWVA>2.0.CO;2.

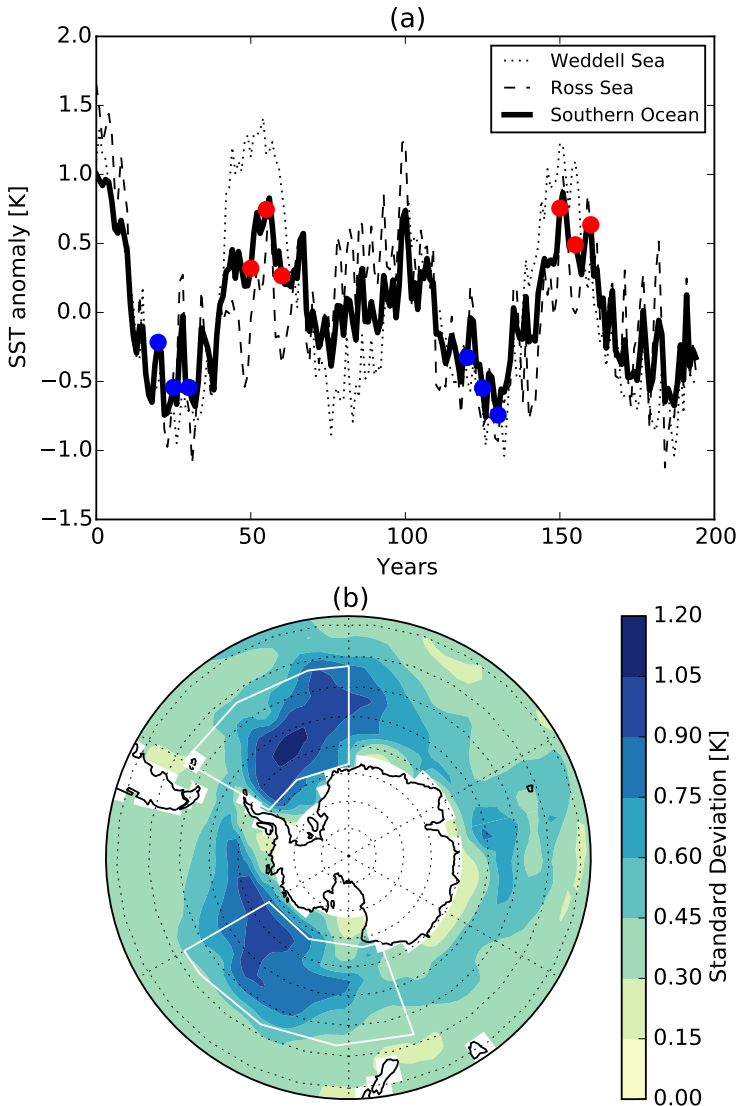
411 LIST OF FIGURES

412	Fig. 1. (left) Seasonal cycle of polar cap (70-90°S) averaged column ozone in the control simulation (1860 SPARC) and the perturbation simulations with year 2000 ozone prescribed with monthly- and daily-mean values from WACCM-SD. (right) Difference of 2000 ozone and 413 1860 ozone simulations.	22
414		
415		
416	Fig. 2. (a) Annual-mean Southern Ocean (50-70°S), Ross Sea (50-75°S, 160°E-120°W), and Wed- 417 dell Sea (50-75°S, 60-0°W) averaged SST from the preindustrial control simulation. Red 418 dots show the initialization dates for the ‘warm start’ ozone depletion simulations and blue 419 dots show the ‘cold start’ initialization dates. (b) Interannual standard deviation of SST from 420 the same simulation. White boxes show the Ross Sea and Weddell Sea regions.	23
421		
422		
423		
424		
425		
426		
427	Fig. 3. (a) Annual average zonal-mean zonal wind stress anomalies, averaged over the 48 years of 428 the ozone perturbation simulations, for the ensemble mean, cold and warm start ensembles, 429 and daily and monthly mean ozone ensembles. Vertical dashed line shows the location of 430 maximum wind stress in the control simulation. (b) Variation of zonal-mean zonal wind- 431 stress with time for the ensemble mean. (c) Zonal wind stress anomalies (colors) and cli- 432 matology from the control simulation (black contours). The contour interval is 50 mPa, and 433 anomalies are calculated relative to the control simulation.	24
434		
435		
436		
437	Fig. 4. Ensemble mean zonal mean SST response. Anomalies are calculated relative to the control 438 simulation.	25
439		
440		
441	Fig. 5. Ocean potential temperature anomaly for the ensemble mean averaged over the Southern 442 Ocean 50°-70°S. The black line shows the mixed-layer depth.	26
443		
444		
445	Fig. 6. (a) Ensemble average, annual-mean Eulerian MOC streamfunction response, Ψ'_{Eul} (Sv, 446 black), and potential temperature, Θ (K, color). The contour interval is 2 K for tempera- 447 ture, and 0.25 Sv for the streamfunction. Solid lines denote a clockwise circulation, dashed 448 counterclockwise. (b) Annual-mean response of the Eulerian (Ψ'_{Eul} , solid) and residual mean 449 (Ψ'_{Res} , dashed) MOC at 200 m, showing the ensemble average as well as daily and monthly 450 ozone ensembles.	27
451		
452	Fig. 7. Annual mean temperature anomaly at 62°S, 200 m for the daily- and monthly-mean ozone 453 simulations as well as the ensemble average. Anomalies are calculated relative to the climati- 454 ology of the control simulation. The dashed line shows the linear best fit to the ensemble 455 average, and the horizontal line represents the value of the ensemble mean SST anomaly 456 between 50-70°S over the first 20 years.	28
457		
458		
459	Fig. 8. Southern Ocean (50-70S) SST anomaly relative to the pre-ozone depletion control simula- 460 tion from the response function runs, split into daily- and monthly-mean ozone and warm 461 and cold start ensembles. SST evolution is dominated by the initial state.	29
462		
463		
464	Fig. 9. Southern Ocean (50-70S) average SST following 10 warm (red) and 11 cold (blue) years 465 sampled from a 500-year control simulation. Shaded regions represent the 95% confidence 466 interval on the expected response calculated from the autocorrelation function. Years are 467 selected from the control simulation which are at least one standard deviation from the mean 468 and spaced at least 5 years apart, in order to mirror the selection of start dates for the ozone 469 response simulations.	30
470		
471		
472	Fig. 10. (a,c,e) Response of Southern Ocean, Ross Sea, and Weddell Sea SST to the ozone pertur- 473 bation. Year zero represents the initial conditions, and year one is the first year after the 474	
475		

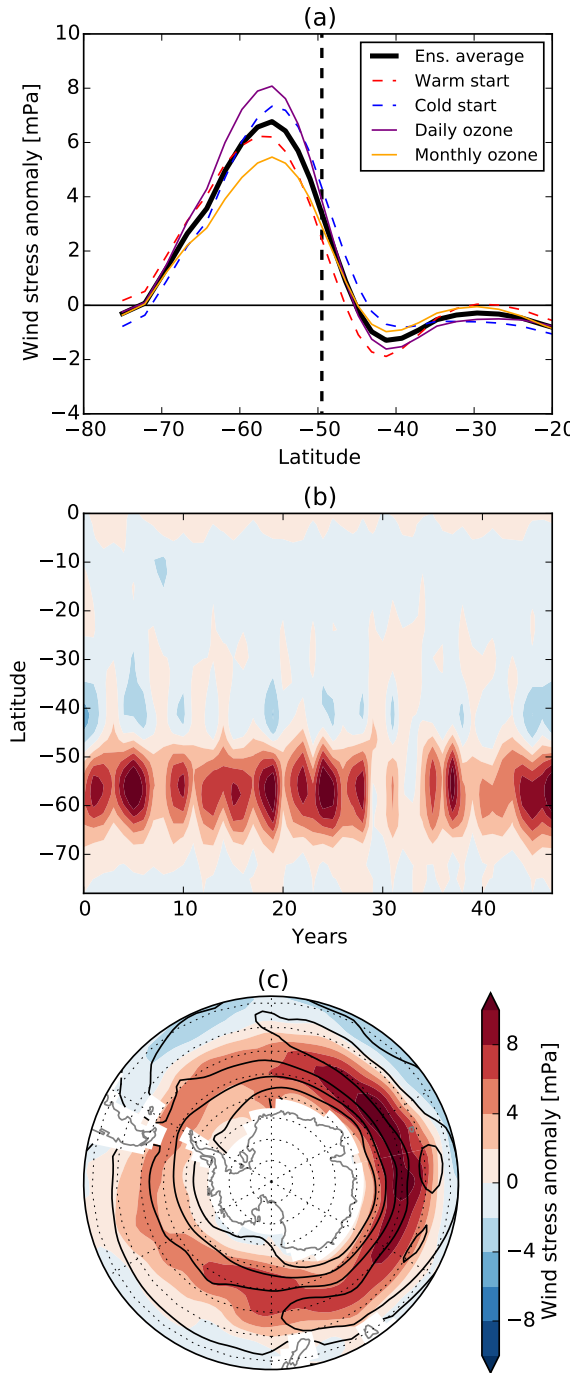
454	perturbation is applied. The shaded region represents the 95% confidence interval on the	31
455	expected response in the absence of a perturbation, calculated from the autocorrelation of	
456	a 500-year control simulation. (b,d,f) Differences of the simulated response from this ex-	
457	pected natural variability.	
458	Fig. 11. SST anomaly of the ensemble mean perturbation simulations relative to the pre-ozone deple-	
459	tion control simulation, for 0-15, 15-30, and 30-45 years following ozone depletion. Gray	32
460	boxes show the Ross and Weddell Sea regions.	
461	Fig. 12. Winter (July-August) sea ice anomaly of the ensemble mean perturbation simulations rela-	
462	tive to the pre-ozone depletion control simulation, for 0-15, 15-30, and 30-45 years follow-	
463	ing ozone depletion.	33
464	Fig. 13. Sea ice anomaly of the ensemble mean perturbation simulations relative to the pre-ozone	
465	depletion control simulation.	34



466 FIG. 1. (left) Seasonal cycle of polar cap ($70\text{--}90^{\circ}\text{S}$) averaged column ozone in the control simulation (1860
 467 SPARC) and the perturbation simulations with year 2000 ozone prescribed with monthly- and daily-mean values
 468 from WACCM-SD. (right) Difference of 2000 ozone and 1860 ozone simulations.



469 FIG. 2. (a) Annual-mean Southern Ocean ($50\text{--}70^{\circ}\text{S}$), Ross Sea ($50\text{--}75^{\circ}\text{S}$, $160^{\circ}\text{E}\text{--}120^{\circ}\text{W}$), and Weddell Sea
 470 ($50\text{--}75^{\circ}\text{S}$, $60\text{--}0^{\circ}\text{W}$) averaged SST from the preindustrial control simulation. Red dots show the initialization
 471 dates for the ‘warm start’ ozone depletion simulations and blue dots show the ‘cold start’ initialization dates. (b)
 472 Interannual standard deviation of SST from the same simulation. White boxes show the Ross Sea and Weddell
 473 Sea regions.



474 FIG. 3. (a) Annual average zonal-mean zonal wind stress anomalies, averaged over the 48 years of the ozone
 475 perturbation simulations, for the ensemble mean, cold and warm start ensembles, and daily and monthly mean
 476 ozone ensembles. Vertical dashed line shows the location of maximum wind stress in the control simulation.
 477 (b) Variation of zonal-mean zonal windstress with time for the ensemble mean. (c) Zonal wind stress anomalies
 478 (colors) and climatology from the control simulation (black contours). The contour interval is 50 mPa, and
 479 anomalies are calculated relative to the control simulation.²⁴

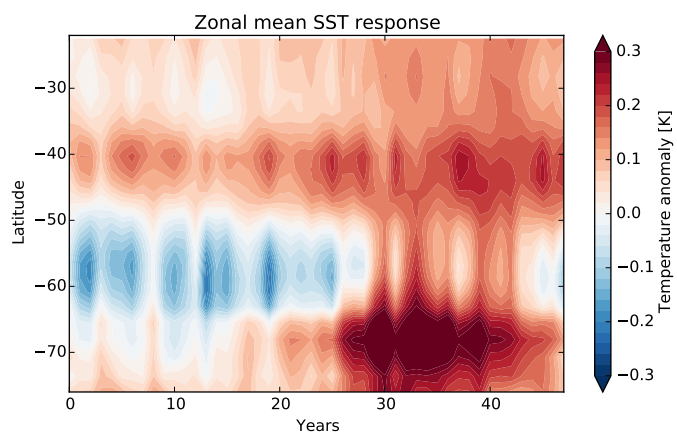
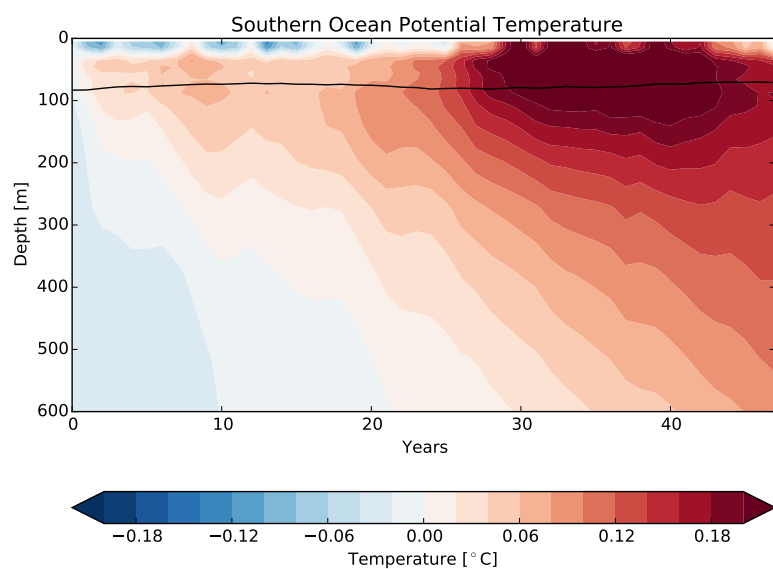
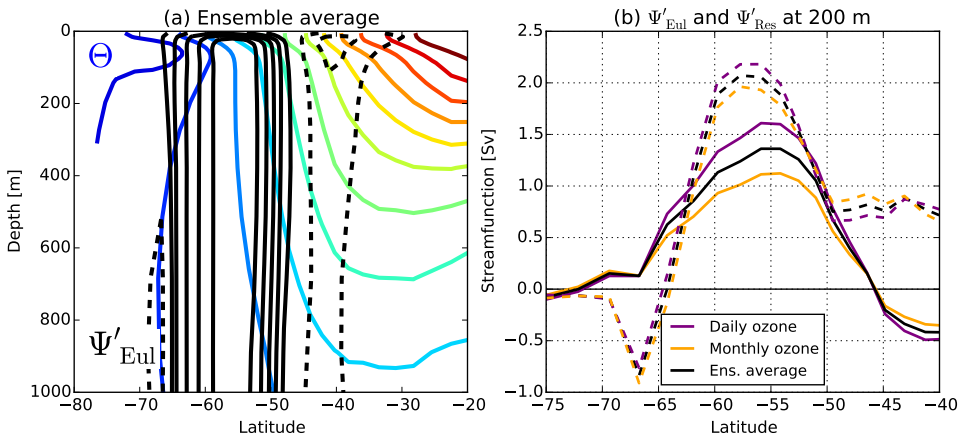


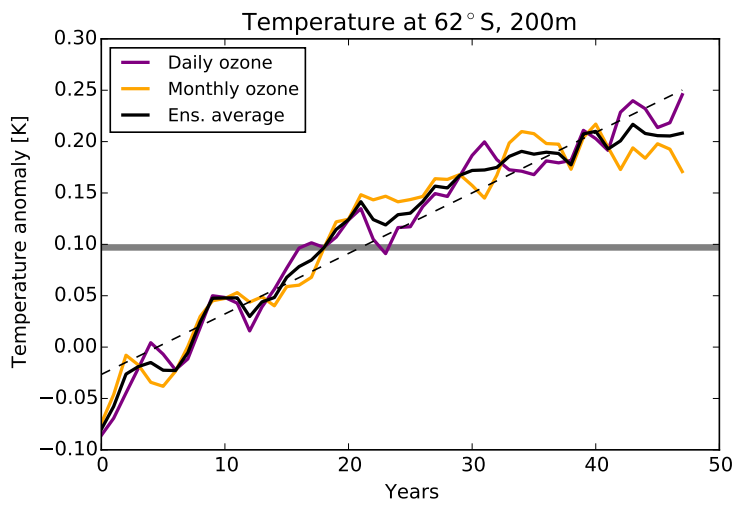
FIG. 4. Ensemble mean zonal mean SST response. Anomalies are calculated relative to the control simulation.



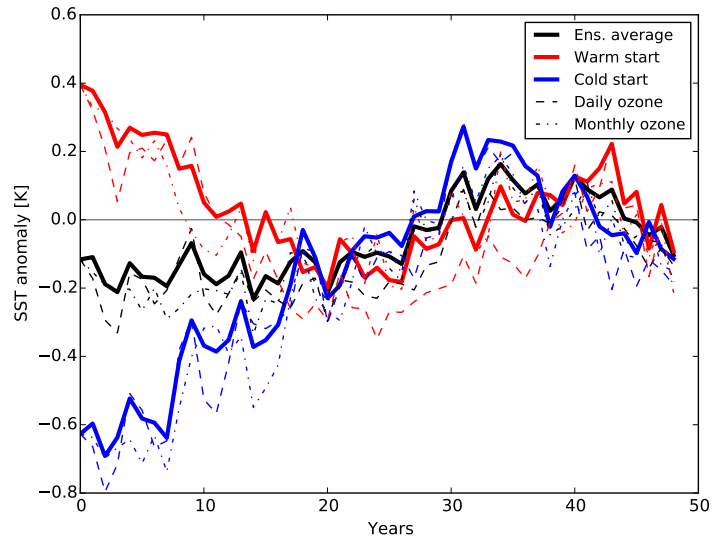
480 FIG. 5. Ocean potential temperature anomaly for the ensemble mean averaged over the Southern Ocean
481 50°-70°S. The black line shows the mixed-layer depth.



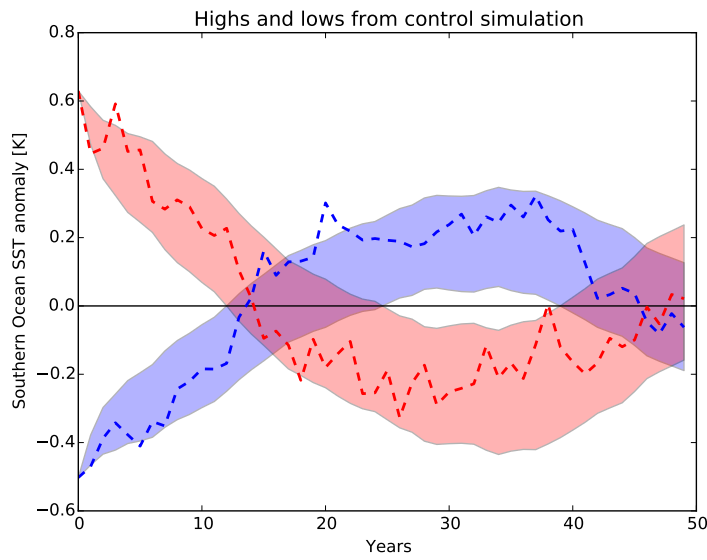
482 FIG. 6. (a) Ensemble average, annual-mean Eulerian MOC streamfunction response, Ψ'_{Eul} (Sv, black), and
483 potential temperature, Θ (K, color). The contour interval is 2 K for temperature, and 0.25 Sv for the stream-
484 function. Solid lines denote a clockwise circulation, dashed counter-clockwise. (b) Annual-mean response of the
485 Eulerian (Ψ'_{Eul} solid) and residual mean (Ψ'_{Res} , dashed) MOC at 200 m, showing the ensemble average as well as
486 daily and monthly ozone ensembles.



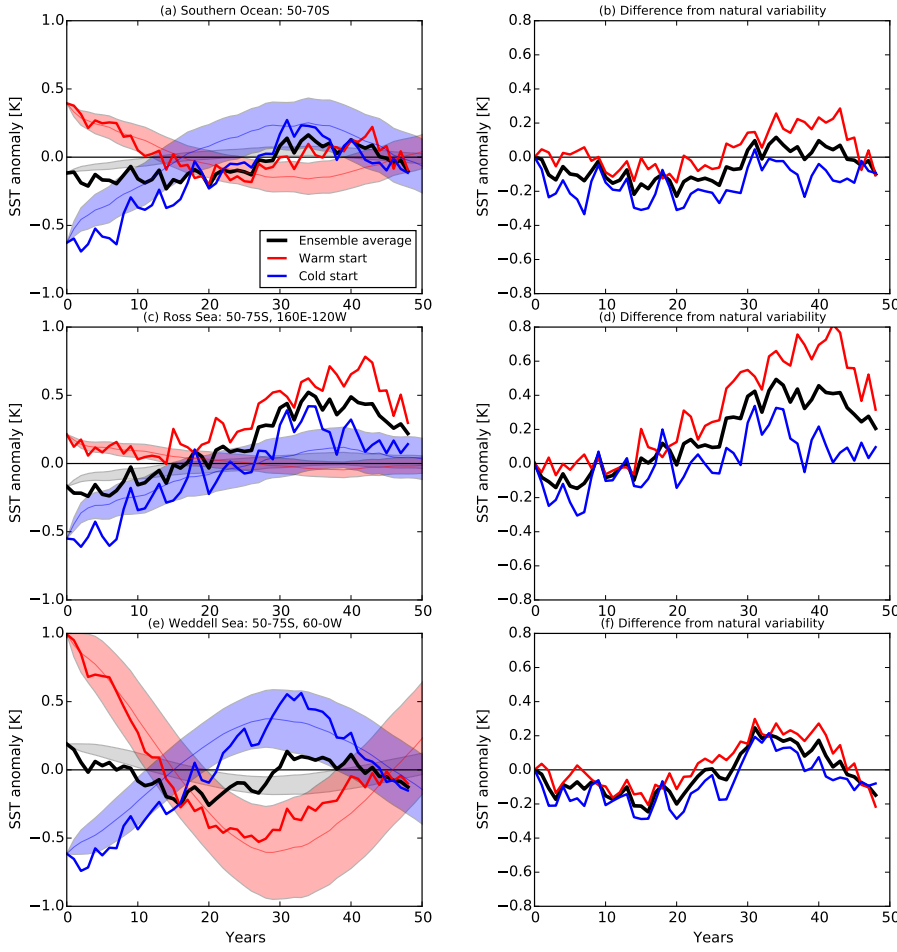
487 FIG. 7. Annual mean temperature anomaly at 62°S, 200 m for the daily- and monthly-mean ozone simulations
 488 as well as the ensemble average. Anomalies are calculated relative to the climatology of the control simulation.
 489 The dashed line shows the linear best fit to the ensemble average, and the horizontal line represents the value of
 490 the ensemble mean SST anomaly between 50-70°S over the first 20 years.



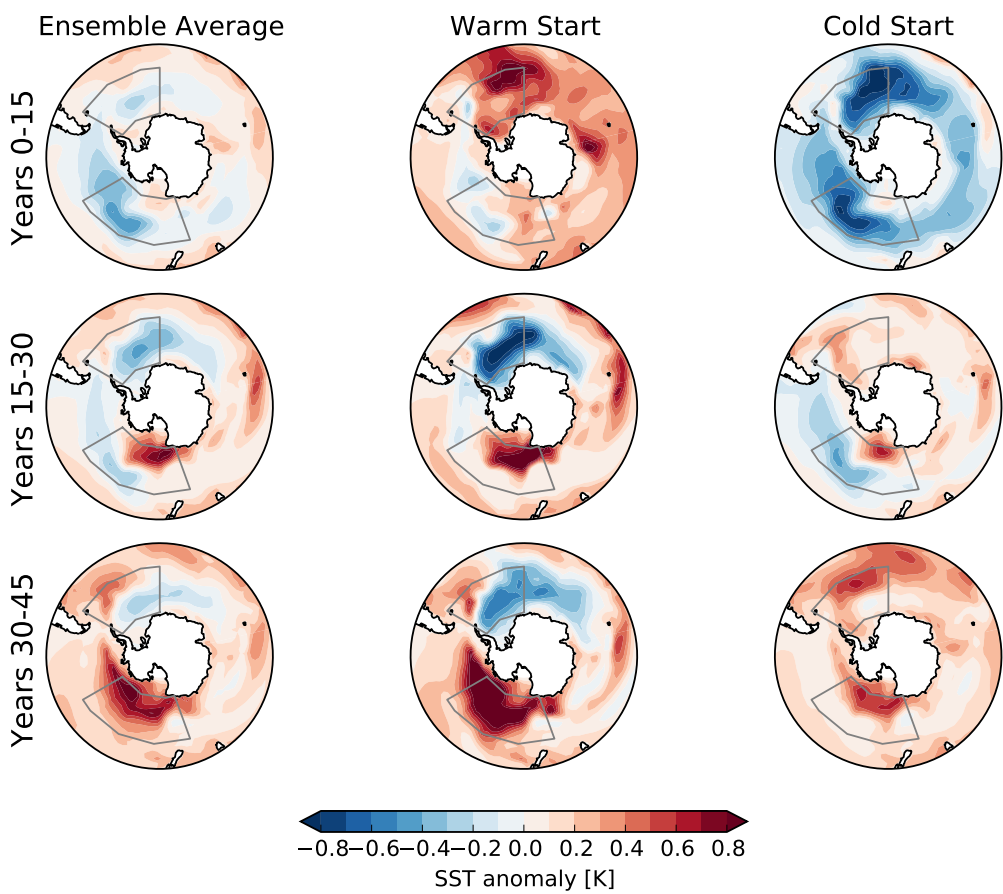
491 FIG. 8. Southern Ocean (50-70S) SST anomaly relative to the pre-ozone depletion control simulation from
 492 the response function runs, split into daily- and monthly-mean ozone and warm and cold start ensembles. SST
 493 evolution is dominated by the initial state.



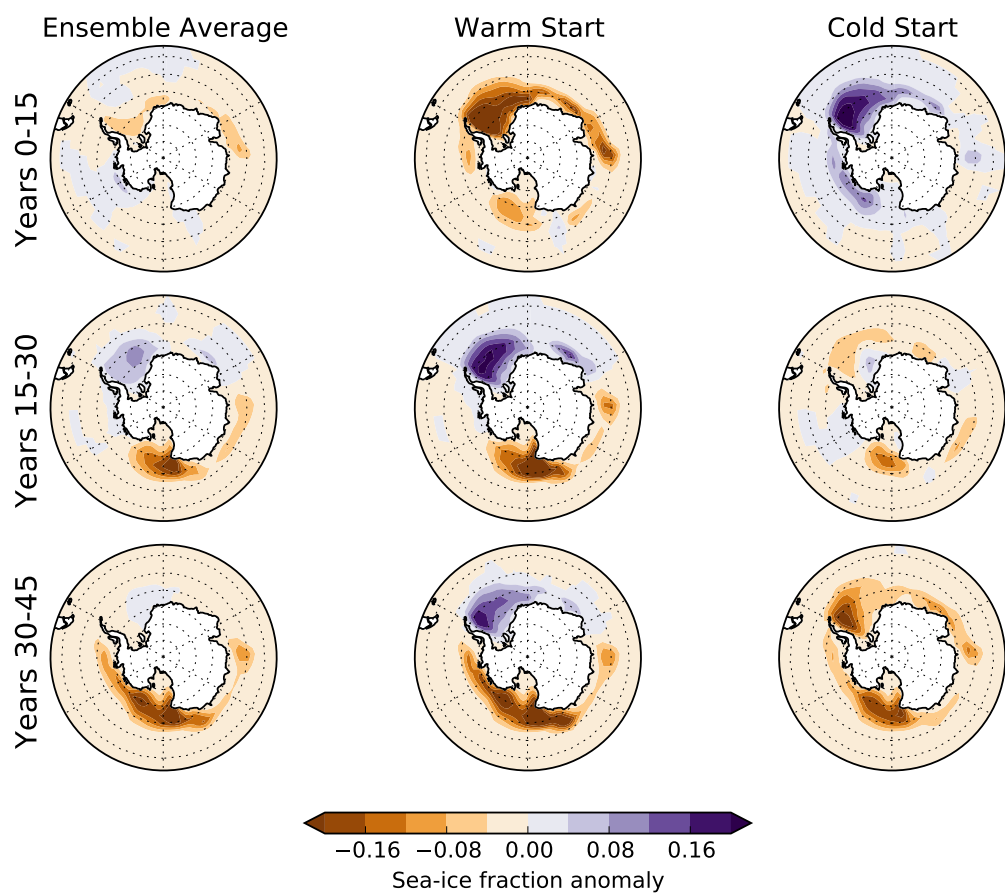
494 FIG. 9. Southern Ocean (50-70S) average SST following 10 warm (red) and 11 cold (blue) years sampled from
 495 a 500-year control simulation. Shaded regions represent the 95% confidence interval on the expected response
 496 calculated from the autocorrelation function. Years are selected from the control simulation which are at least
 497 one standard deviation from the mean and spaced at least 5 years apart, in order to mirror the selection of start
 498 dates for the ozone response simulations.



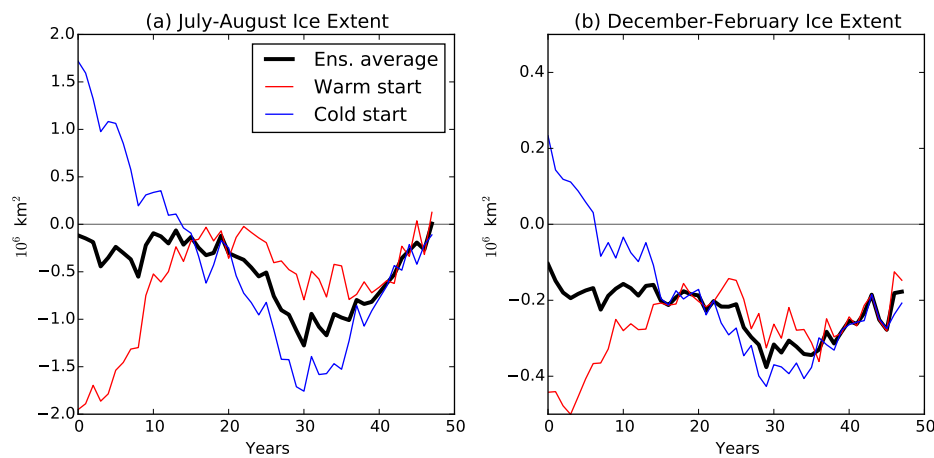
499 FIG. 10. (a,c,e) Response of Southern Ocean, Ross Sea, and Weddell Sea SST to the ozone perturbation. Year
 500 zero represents the initial conditions, and year one is the first year after the perturbation is applied. The shaded
 501 region represents the 95% confidence interval on the expected response in the absence of a perturbation, calcu-
 502 lated from the autocorrelation of a 500-year control simulation. (b,d,f) Differences of the simulated response
 503 from this expected natural variability.



504 FIG. 11. SST anomaly of the ensemble mean perturbation simulations relative to the pre-ozone depletion
 505 control simulation, for 0-15, 15-30, and 30-45 years following ozone depletion. Gray boxes show the Ross and
 506 Weddell Sea regions.



507 FIG. 12. Winter (July-August) sea ice anomaly of the ensemble mean perturbation simulations relative to the
 508 pre-ozone depletion control simulation, for 0-15, 15-30, and 30-45 years following ozone depletion.



509 FIG. 13. Sea ice anomaly of the ensemble mean perturbation simulations relative to the pre-ozone depletion
510 control simulation.